14

Ordered Semiconductor Photoanode Films for Dye-Sensitized Solar Cells Based on Zinc Oxide-Titanium Oxide Hybrid Nanostructures

Xiang-Dong Gao, Cai-Lu Wang, Xiao-Yan Gan and Xiao-Min Li
State Key Lab of High Performance Ceramics and Superfine Microstructures, Shanghai Institute of Ceramics, Chinese Academy of Sciences, Shanghai, P. R. China

1. Introduction

Dye-sensitized solar cell (DSC) is a new type solar cell based on the photoelectric conversion occurred at the organic dye-semiconductor nanoparticle interface. DSC has attracted great research interests due to its high efficiency for energy conversion (11%) and low production cost compared with the traditional Si based photovoltaic cell (O'Regan et al., 1991; Grätzel et al., 2001). In confront of the huge difficulties in propelling the conversion efficiency of DSC up to 15% or higher, very recently, significant research efforts have been redirected to the optimization of photoanode, while others are stick to seeking better sensitizer or solid electrolytes (Mor et al., 2006a; Grätzel et al., 2006; Li et al., 2006; Zhang et al., 2011).

The photoanode is the kernel component of DSC assuming two major functions, supporting dye molecules, and transporting photo-induced electrons to the bottom electrode. Traditionally, the photoanode is the nanoporous thick film (15-20 um in thickness) consisted of TiO_2 nanoparticles, characterized by the disordered nature (Figure 1a). The electron transport in this disordered network of TiO_2 film is rather difficult due to two factors: (1) The presence of a large quantity of electron traps at the nanostructured TiO_2/electrolyte interface, such as the intrinsic defect sites (e.g. oxygen defects or surface states) and the grain boundaries, which may influence the interfacial charge-transfer kinetics. (2) The tortuosity of the electron path in the photoanode formed via the calcinations at high temperature, which may hinder the free transport of electron and increase the electron-hole recombination rate. In contrast, the ideal photoanode film (Figure 1b) should be built up by very thin (10-20 nm) and long (10-20 um) semiconductor nanowire array, possessing no surface states, which should exhibit the total photoelectric conversion efficiency of 24% based on the widely used black dye (N719) and I^2/I^{3-} electrolyte system. However, limited by the current fabrication technology level, it is extremely difficult to realize this photoanode film in a short term. Therefore, the development of some practical measures to optimize the photoanode is fundamentally important. The photoanode film can be optimized further from two aspects, to enhance electron gathering and transporting efficiency and to inhabit the charge recombination at the same time. Figure 1c illustrates the schematic of the hybrid photoanode structure, using 1D ZnO nanowire as the major path for the electron transportation, and using 0D TiO_2 nanoparticles as the supporting framework of dye molecules. By using two kinds of nanostructures assuming two different functions of

the photoanode, the efficiency of the hybrid photoanode is expected to improve compared with the traditional nanoparticle-based photoanode.

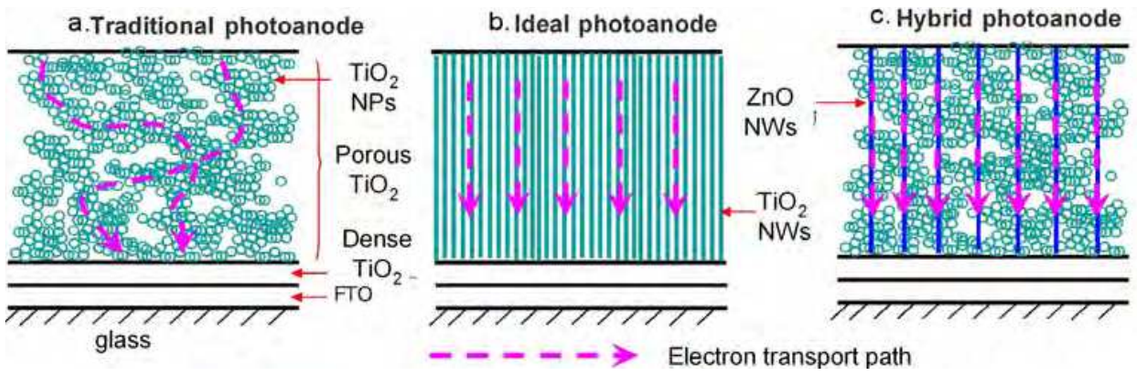

Fig. 1. Schematic of the electron transporting path in the traditional, ideal, and hybrid photoanode. NPs: Nanoparticles; NWs: Nanowires.

Many efforts have been devoted to construct photoanodes of DSCs using ordered semiconductor nanostructures such as nanowires, nanotubes or hierarchical structures. In 2005, M. Law et al. first demonstrated the photoanode film built by a dense array of oriented and crystalline ZnO nanowires (Law et al., 2005). The direct electrical pathways provided by the nanowires ensured the rapid collection of carriers generated throughout the device, and a full Sun efficiency of 1.5% was demonstrated, limited primarily by the surface area of the nanowire array. G. K. Mor et al. reported highly ordered transparent TiO_2 nanotube arrays (6-nm pore diameter, 17-nm wall thickness, and 360-nm length) as the photoanode, which were grown perpendicular to a fluorine-doped tin oxide-coated glass substrate by anodic oxidation of a titanium thin film (Mor et al., 2006b). Although the electrode was only 360-nm-thick, the generated photocurrent was 7.87 mA/cm², with a photocurrent efficiency of 2.9%, indicating the great potential of the ordered photoanode. K. Zhu et al. investigated the dynamics of electron transport and recombination in DSCs incorporating oriented TiO_2 nanotube arrays from electrochemically anodized Ti foils, and proved that the nanotube-based DSCs had significantly higher charge-collection efficiencies than the nanoparticle-based counterparts (Zhu et al., 2007). S H Kang et al. developed chemically synthesized TiO_2 nanorod based photoanodes (Kang et al., 2008). These nanorod-based DSCs showed improved photovoltaic properties (6.2 % versus 4.3 % for nanoparticle-based DSCs) owing to the characteristics of slightly enhanced electron transport and predominantly degraded charge recombination. W. Zhang et al. used mesoporous TiO_2 nanofibers with a high surface area of 112 m² /g prepared by electrospinning technique as the photoanode, and demonstrated the conversion efficiency of 1.82% in solid-state DSCs (Zhang et al., 2010). Recently, C. S. Rustomji et al. designed and constructed photoanodes based on new 3-D configurations of TiO_2 nanotubes, which, unlike prior nanotube-based cells where tubes were grown vertically in a 2-D array, consisted of tubes that extended radially in a 3-D array from a grid of fine titania wires (Rustomji et al., 2010). Its overall efficiency reached 5.0%, and the incident photon-to-current efficiency exceeds 60% over a broad part of the visible spectrum. S. Guldin et al. presented a material assembly route toward double-layer photoanode of DSCs, by coupling a high-surface mesoporous underlayer with an optically and electrically active three-dimensionally periodic TiO_2 photonic crystal overlayer (Guldin et al., 2010). In contrast to earlier studies, the double layer structure exhibited porosity at the mesoporous and the microporous length scales as well as pore and electronic connectivity at

all levels. This construct enabled effective dye sensitization, electrolyte infiltration and charge collection from both the mesoporous and the photonic crystal layers.

Apart from various ordered TiO_2 nanostructures, ZnO has also been widely investigated as an alternative of TiO_2 to construct the photoanode of DSCs. For example, E. Hosono et al. pyrolyzed upright-standing sheets of layered hydroxide zinc carbonate, and obtained upstanding nanocrystalline ZnO films with the *c*-axis parallel to the substrate (Hosono et al., 2005). The corresponding DSCs possessed the conversion efficiency of 3.9%, much higher than the regular efficiency level of ~2% at that time (Rensmo et al., 1997). C. K. Xu et al. reported the photoanode using ultralong ZnO nanowires with up to 33 μm thick sensitizing films while maintaining high electron collection efficiency, which resulted in greatly improved performance (from 1.1% to 2.1%) compared to previously reported ZnO nanowire-based DSCs (Xu et al., 2010). J. X. Wang et al. used porous hierarchical disklike ZnO nanostructure fabricated via a simple low-temperature hydrothermal method as the photoanodes, and achieved improved photovoltaic performance (2.49%) compared with that of the ZnO nanowire arrays owing to the enlarged surface area and natural electron collection routes of ZnO hierarchical nanostructures (Wang et al., 2010). A. B. F. Martinson et al. introduced high surface area ZnO nanotube photoanodes templated by anodic aluminum oxide in DSCs via atomic layer deposition technique, providing a direct path for charge collection over tens of micrometers thickness (Martinson et al., 2007). Compared to similar ZnO-based devices, ZnO nanotube cells show exceptional photovoltage and fill factors, in addition to power efficiencies up to 1.6%. G Z Cao's group took the hierarchically popcorn-ball structured ZnO film as the photoanode, and attained the efficiency improvement from 0.6% to 3.5%, and finally 5.4%, by inducing light scattering within the photoelectrode films via the aggregation of ZnO nanocrystallites, thus demonstrating the huge potential of ZnO nanostructures in realizing DSCs with high efficiency (Chou et al., 2007; Zhang et al., 2008).

In parallel with photoanode films consisted by merely one type of material (ZnO, TiO_2, nanoparticles, nanowires, or nanotubes), the hybrid photoanode represents another important research trend, which is usually built by two or more materials or morphologies. Due to the obvious advantages of the hybrid photoanode including the improved interfacial structure/charge separation, the direct electron transporting path, and the vast possibilities to tune the microstructure and photoelectrochemical properties of the photoanode, this research trend has been gaining more and more interests. For example, K. M. Lee et al. incorporated multi-wall carbon nanotube in low-temperature fabricated TiO_2 photoanode, with the efficiency improvement of 20% (0.1% CNT), which may be resulted from retarded charge recombination between injected electrons and electron acceptors in the redox electrolyte (Lee et al., 2008). P. Brown et al. studied the single-wall carbon nanotube (SWCNT)/TiO_2 hybrid system, and proved that SWCNT support networks can be incorporated into mesoscopic TiO_2 films to improve the charge transport in DSCs (Brown et al., 2008). While no net increase in power conversion efficiency was obtained, an increase in photon-to-current efficiency (IPCE) represented the beneficial role of the SWCNT as a conducting scaffold to facilitate charge separation and charge transport in nanostructured semiconductor films. S. Pang et al. incorporated ZnO nanorods with different sizes into TiO_2 nanoparticle-based photoanode, and improved the conversion efficiency by 15% (Pang et al., 2007). They attributed the improved efficiency to the faster charge carrier transport rate, the decreased recombination, and the higher V_{oc}. B. Tan et al. used the composites of anatase TiO_2 nanoparticles and single-crystalline anatase TiO_2 nanowires as electrodes to fabricate DSCs, which possessed the advantages of both building blocks, i.e., the high surface area of

nanoparticle aggregates and the rapid electron transport rate and the light scattering effect of single-crystalline nanowires (Tan et al., 2006). An enhancement of power efficiency from 6.7% for pure nanoparticle cells to 8.6% for the composite cell with 20 wt% nanowires was achieved, showing that employing nanoparticle/nanowire composites represented a promising approach for further improving the efficiencies of DSCs. C. H. Ku et al. reported ZnO nanowire/nanoparticle composite photoanodes with different nanoparticle-occupying extents (Ku et al., 2008). Aligned ZnO nanowires were grown on the seeded FTO substrate using an aqueous chemical bath deposition (CBD) first, and then, growth of nanoparticles among ZnO NWs by another base-free CBD was preceded further for different periods. The corresponding DSCs showed an efficiency of 2.37%, indicating the good potential of the hybrid nanostructures in ordered photoanodes.

Apart from the direct blending of two different semiconductor components as mentioned above, the coating technique has also been applied widely to create the hybrid photoanodes. M. Law et al. developed photoanodes constructed by ZnO nanowires arrays coated with thin shells of amorphous Al_2O_3 or anatase TiO_2 by atomic layer deposition (Law et al., 2006). They found that, while alumina shells of all thicknesses acted as insulating barriers that improve cell open-circuit voltage only at the expense of a larger decrease in short-circuit current density, titania shells in thickness of 10-25 nm can cause a dramatic increase in V_{OC} and fill factor with little current falloff, resulting in a substantial improvement in overall conversion efficiency (2.25%). They attributed the improved performance to the radial surface field within each nanowire that decreases the rate of recombination. K. Park et al. described a ZnO-TiO_2 hybrid photoanode by coating ultrathin TiO_2 layer by atomic layer deposition on submicrometer-sized aggregates of ZnO nanocrystallites (Park et al., 2010). The introduction of the TiO_2 ultrathin layer increased both the open circuit voltage and the fill factor as a result of the suppressed surface charge recombination without impairing the photocurrent density, thus realizing more than 20% enhancement in the conversion efficiency from 5.2% to 6.3%. S. H. Kang et al. examined effects of ZnO coating on the anodic TiO_2 nanotube array film on the conversion efficiency (Kang et al., 2007). Compared with the solid-sate cells consisted of an anodic TiO_2 film as the working electrode under backside illumination, an almost 20% improvement from the ZnO coating was achieved (from 0.578% to 0.704%), which can be attributed to the suppressed electron flow to the back-direction and the enhanced open-circuit voltage.

Despite considerable effects in this area, however, the record efficiency of 11% for DSCs is not surpassed by these new type cells, due to the complexity of both the nanoporous photoanode and the cell structure of DSCs. Much comprehensive and in-depth work related to this topic is required.

In this chapter, we focused on the ordered photoanode film built up by two semiconductor materials, zinc oxide (ZnO) and titanium oxide (TiO_2). Three type of ZnO nanostructures were selected, including the nanowire array (grown by the hydrothermal method), the nanoporous disk array grown on FTO substrate, and the nanoporous disk powder (transformed from the solution-synthesized zinc-based compound $ZnCl_2.[Zn(OH)_2]_4.H_2O$). Different types of TiO_2 nanoparticles were used, including commercial nanoparticles P25 & P90 (Degauss Co., Germany), and home-made hydrothermal TiO_2 nanoparticles, which have been widely used in producing traditional high-efficiency DSCs. Two kinds of preparation technique of ZnO-TiO_2 hybrid film were used according to the status of ZnO nanostructures (array or powder). The microstructure, optical and electrical properties of the hybrid film were investigated, and the performance of corresponding DSCs was measured and

compared with results of traditional cell. In special, the emphasis was placed on the controlling method of the microstructure of ZnO-TiO_2 hybrid films, and on the electron transporting mechanism in the hybrid films.

2. ZnO nanowire array/TiO_2 NPs hybrid photoanodes

In this section, two types of ZnO nanowire (NW) array were selected, i.e., dense and sparse NW array, with an aim to examine the effects of the distribution density of NW on the microstructure and photoelectrochemical properties of the hybrid cells. For the dense NW array, the ultrasonic irradition was used to promote the penetration of TiO_2 nanoparticles in the interstice of ZnO NWs.

2.1 Hybrid photoanodes based on dense ZnO NW array

ZnO nanowire (NW) arrays were grown on ZnO-seeded fluorinated tin oxide (FTO, 20 Ω/□) substrates by chemical bath deposition method. ZnO seed layer was prepared by sol–gel technique. ZnO NW arrays were obtained by immersing the seeded substrates upside-down in an aqueous solution of 0.025 mol/L zinc nitrate hydrate and 0.025 mol/L hexamethylenetetramine (HMT) in a sealed beaker at 90 °C for 12 h. After the deposition of ZnO NW, TiO_2 nanoparticles (NPs) were coated on ZnO NW by dipping the substrate into a well-dispersed TiO_2 suspension containing 0.5 g TiO_2 NPs (P25), 20 μL acetyl acetone, 100 μL Triton X-100 in 10 mL distilled water and 10 mL ethanol with 20 μL acetic acid. To facilitate the attachment and the gap filling of TiO_2 NPs into the interstices of ZnO NWs, the ultrasonic irradiation generated from a high-density ultrasonic probe (Zhi-sun, JYD-250, Ti alloy-horn, 20–25 kHz) was applied to TiO_2 suspension. The working mode was adjusted to work for 2 seconds and idle for 2 seconds, with the repetition of 99 cycles. The electrodes were then withdrawn at a speed of 3 cm per minute, dried, and sintered at 450 °C for 30 min in air. Figure 2 gave the schematic for the fabrication of the hybrid ZnO NW array/TiO_2 photoanopde.

For DSCs fabrication, ZnO NW based electrodes were immersed in a 0.5 mmol/L ethanol solution of N719 for 1 h for dye loading. The sensitized electrode was sandwiched with platinum coated FTO counter electrode separated by a hot–melt spacer (100 μm in thickness, Dupont, Surlyn 1702). The internal space of the cell was filled with an electrolyte containing 0.5 mol/L LiI, 0.05 mol/L I_2, 0.5mo/L 4-tertbutylpyridine, and 0.6 mol/L 1-hexyl-3-methylimidazolium iodide in 3-methoxypropionitrile solvent. The active cell area was typically 0.25 cm^2.

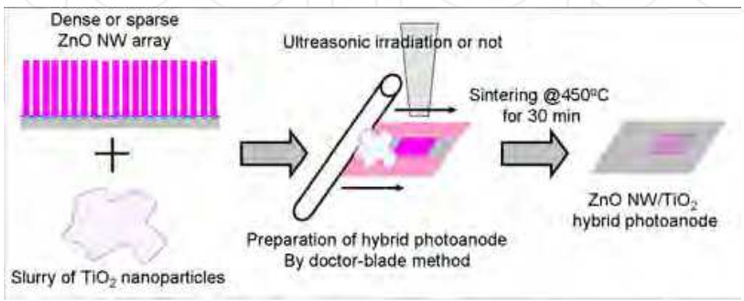

Fig. 2. Schematic of the preparation process of ZnO NW array/TiO_2 nanoparticles hybrid photoanode. NW: Nanowire.

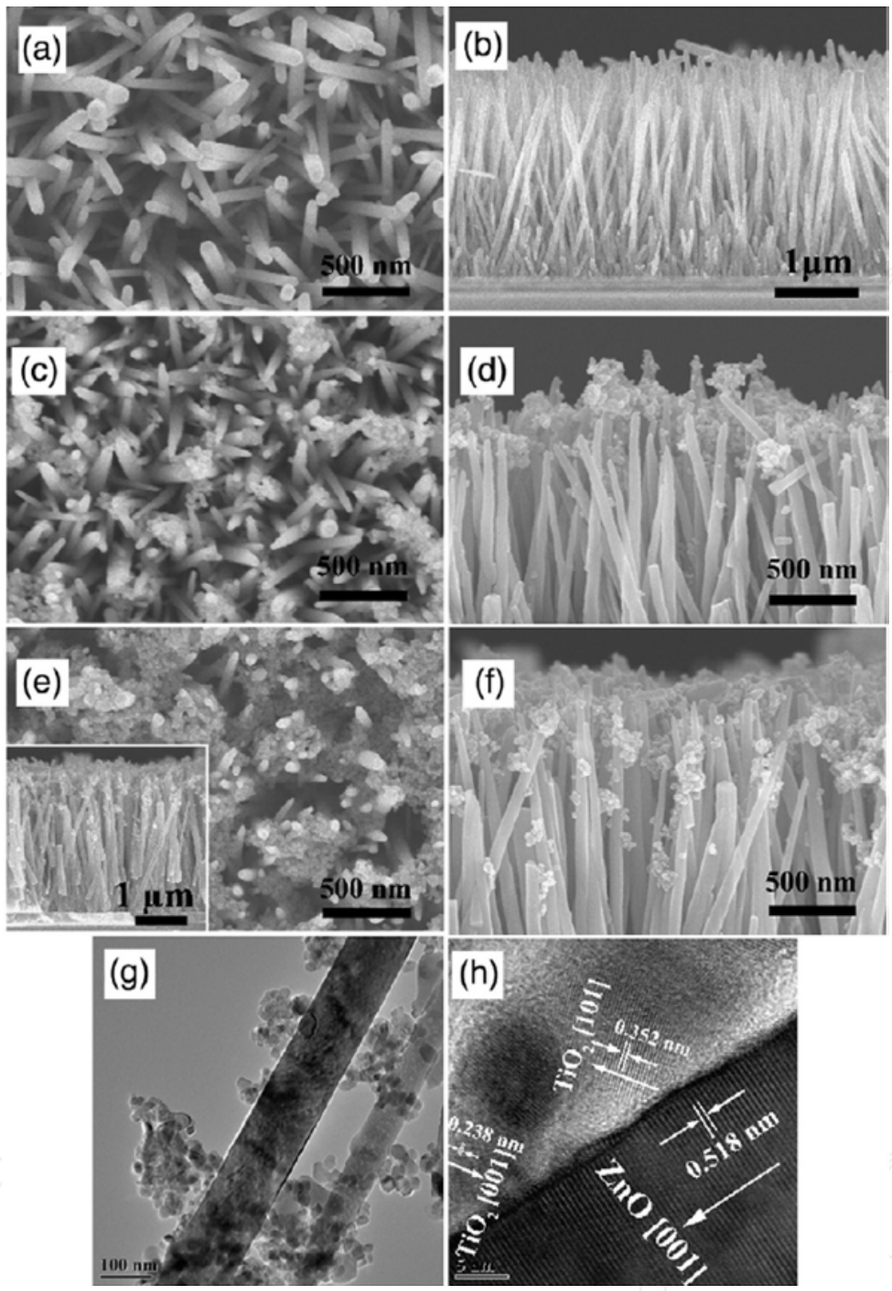

Fig. 3. FESEM images of ZnO NW arrays (a)–(b), hybrid ZnO NW/TiO_2 NP photoanodes prepared without (c)–(d), and with (e)–(f) the ultrasonic treatment. (g) Low and (f) high-resolution TEM images of the hybrid photoanodes prepared with ultrasonic treatment. (Reproduced from Ref. (Gan et al., 2007))

Figure 3 showed the top and side-view SEM images of ZnO NWs grown on FTO substrate and ZnO-TiO_2 hybrid photoanode film with/without ultrasonic treatment. Results indicate that, for ZnO nanowire array with a density of ~3.3×10^9 cm^{-2} and an average diameter of 80 nm and length of 3 μm, TiO_2 slurry with relatively high viscosity is difficult to penetreate into the inner pore of ZnO nanowires. As can be seen from Fig.3 c and d, only a small

amount of TiO_2 NPs were covered on the side surface of NWs and most of the NPs sit on the top of NWs without filling in the inner gaps. When the ultrasonic irradiation was applied, the coverage of NPs on the side surface of NWs was significantly improved (Fig. 3 e-h), and TiO_2 NPs were uniformly infiltrated into the interstices of NWs rather than stuck to the top of NWs. The cavitation in liquid–solid systems induced by the ultrasonic irradiation bears intensive physical effects, which can promote the transfer of TiO_2 NPs and drive them infiltrating into the gaps of NPs.

Figure 4 (left) showed the absorption spectra of the N719-sensitized ZnO NW, and hybrid ZnO NW/TiO_2 NP electrodes prepared with and without ultrasonic treatment, respectively. The absorption peak at around 515 nm, which corresponded to metal to ligand charge transfer (MLCT) in N719 dye (Nazeeruddin et al., 1993), significantly increased for the hybrid electrodes as compared to that of the pure ZnO NW electrode, proving that the dye-loading content is apparently increased upon the combination of ZnO NW with TiO_2 NPs. Besides, the hybrid electrode prepared with ultrasonic treatment showed an increase in the absorption in the wavelength range of 400–800 nm compared with that without ultrasonic treatment, indicating the higher surface area and the enriched light harvesting property by filling more TiO_2 NPs into the interstices between ZnO NWs with the assistance of ultrasonic irradiation.

Figure 4 (right) illustrated I–V characteristics of DSCs based on pure ZnO NWs and ZnO/TiO_2 hybrid photoanodes. Results show that the short-circuit current density (I_{sc}) and the conversion efficiency (η) of ZnO NWs based cell can be dramatically improved by incorporating TiO_2 NPs, which can be ascribed to the increase in the surface area and the dye loading quantity. However, the open-circuit voltage (V_{oc}) and the fill-factor (FF) of the hybrid DSCs decreased compared to those of pure ZnO NW DSC, which may be resulted from the increased interfaces and surface traps in the hybrid photoanode which may act as the recombination center under illumination. For the hybrid photoanode prepared with ultrasonic treatment, its I_{sc}, V_{oc}, FF, and η was 3.54 mA/cm², 0.60 V, 0.37, and 0.79%, respectively, indicating an approximately 35% improvement of the overall conversion efficiency compared with the photoanode without ultrasonic treatment. This improvement may originate from the enhanced light harvesting and the better attachment of TiO_2 NPs to ZnO NWs resulted from the efficient pore filling induced by the ultrasonic irradiation treatment.

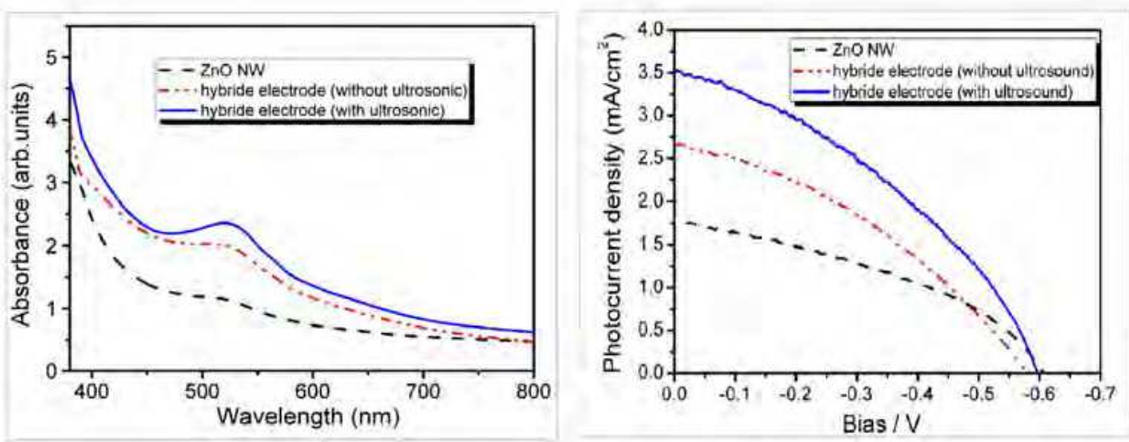

Fig. 4. The absorption spectra (left) of N719-sensitized ZnO NW arrays, and hybrid ZnO NW/TiO_2 NP photoanodes prepared without and with ultrasonic treatment, and I–V characteristics of corresponding DSCs (right). (Reproduced from Ref. (Gan et al., 2007))

In summary, these results indicate that, for the hybrid films combining dense ZnO NW array and TiO_2 NPs, the crucial aspect is to make TiO_2 NPs contained in the slurry penetrate into the deep interstice of ZnO NWs. The application of ultrasonic irradiation or other external fields may be helpful for the penetration of TiO_2 NPs, which usually result in the increase of the photoelectrochemical performance of the hybrid cells. However, it seems that the full filling of TiO_2 in the dense NW array is very difficult based on the current technique. So it is meaningful to develop the sparse nanowire array or other forms of TiO_2 NPs, to realize the good combination of ZnO NW array and TiO_2 NPs.

2.2 Hybrid photoanodes based on sparse ZnO NW array

In this section, ZnO NW array with sparse density was integrated with TiO_2 NPs, to form the hybrid photoanode. The growth of sparse ZnO NW array was realized by reducing the pH value of the precursor via the chemical bath deposition (CBD) method. The substrates and the experimental parameters were similar to those of dense one except the concentration of Zn^{2+} and HMT (both 0.02 mol/L), and the pH value (2.0-3.0).

TiO_2 slurry was prepared following the method in Ref (Ito et al., 2008), and the mass ratio of TiO_2, ethyl cellulose, and terpineol was 18 : 9 : 73. Due to the acid-dissolute nature of ZnO materials, the pH value of TiO_2 slurry should be controlled neutral or weak alkaline.

The preparation of the hybrid film based on sparse ZnO NW array was similar to that of dense array, as described in Section 2.1. The sensitization of the film was carried out in N719 dye solution dissolved in a mixture of acetonitrile and tertbutyl alcohol (volume ratio, 1:1) for 20-24 hours at room temperature. The fabrication of the cells was similar to the procedure described in Section 2.1, with the electrolyte composition of 0.6 M BMII, 0.03 M I_2, 0.10 M guanidinium thiocyanate and 0.5 M 4-tertbutylpyridine in a mixture of acetonitrile and valeronitrile (volume ratio, 85:15).

Figure 5 gave SEM images of sparse ZnO NW on the surface and cross section. It can be seen that the density of ZnO nanowire on FTO substrate is much sparser than the dense ZnO NW (Figure 3 a&b). But with the decrease of the density, the diameter of ZnO NW increases greatly, up to several micrometers.

The hybrid cell based on the sparse ZnO NW array exhibited the conversion efficiency of 2.16%, lower than the TiO_2 NPs-based cell (2.54%) as illustrated in Figure 6. The decreased efficiency of the hybrid cell is mainly resulted from the reduced photocurrent density compared with the TiO_2 cell, while the open voltage keeps unchanged and the fill factor improved from 0.06 to 0.078. The open-circuit voltage decay (OCVD) analysis (Figure 6) indicated that the hybrid film exhibits longer decay time when the illumination is turned off, indicating lower recombination rate between photo-induced electrons and holes. We believe that the obviously reduced photocurrent density may be related to the reduced surface area induced by the incorporation of large size ZnO nanowires, which may resulted in the reduced dye loading content. So the improvement in the efficiency of DSCs via the integration of sparse ZnO NW array and TiO_2 NPs is possible, as long as the size of ZnO nanowire can be reduced to tens of nanometers. However, limited by the current technology level of ZnO nanowire array, it is not an easy task to grow ZnO NW array both sparse and thin enough for the application in the hybrid photoanodes of DSCs.

In summary, we have successfully prepared the hybrid photoanode film using sparse ZnO

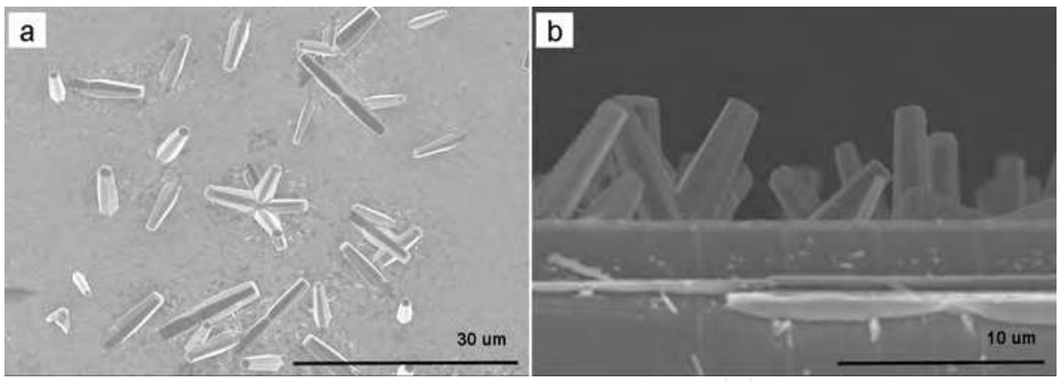

Fig. 5. FESEM images of sparse ZnO NW array on the surface (a) and the cross section (b).

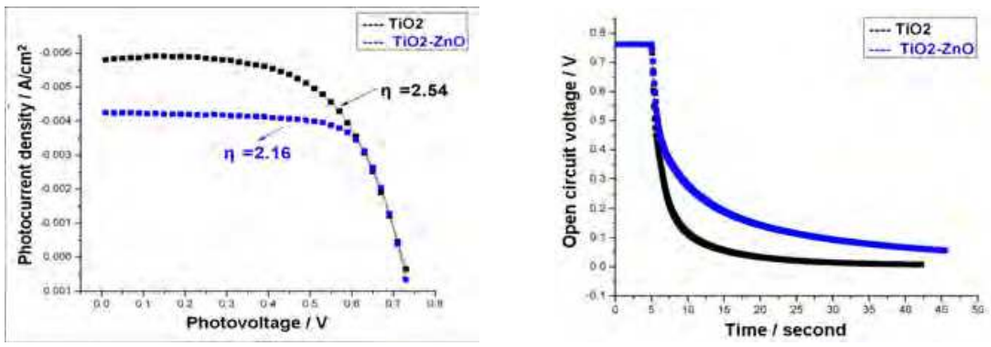

Fig. 6. I-V curves (left) and open-circuit voltage decay (OCVD) curves (right) of TiO_2 NPs-based cell and ZnO–TiO_2 hybrid cells based on sparse ZnO NW array under AM 1.5 illumination (100 mW/cm²). The active area is 0.27 cm² for all cells.

NW array and TiO_2 NPs. Although the total efficiency of the hybrid cell was lower than the TiO_2 NPs-based cell, the obvious improvement in the fill factor and the reduction in the recombination rate were observed. The reduced efficiency was mainly related to the decreased photocurrent density originated from the large-size ZnO NW. The further chance to improve the efficiency of ZnO NW based hybrid cell may reside in the realization of ZnO NWs with both sparse density and thin diameter.

3. ZnO nanoporous disk array/TiO_2 NPs hybrid photoanodes

In this section, an alternative ZnO nanostructure was used to prepare hybrid photoanode film, i.e., ZnO disk array possessing nanoporous feature. Compared with the traditional ZnO NW, the thickness of ZnO disk is lower and the surface area is higher. Thus higher effect in improving the conversion efficiency of DSCs can be expected.

ZnO nanoporous disk array was transformed from the disk of a layered zinc-based compound – simonkollite ($ZnCl_2.[Zn(OH)_2]_4.H_2O$, brief as ZHC) via calcinations. Conductive FTO glass coated by a thin TiO_2 layer (deposited by the hydrolysis of 40 mM $TiCl_4$ aqueous solution at 70°C) was used as the substrate. Typically, ZHC disk was prepared by CBD method. Aqueous solutions of 20 ml $ZnCl_2$ (0.2 mol/l), 20 ml hexamethylenetetramine (HMT) (0.2 mol/l), and 40 ml ethanol were mixed in a beaker and heated to 70°C in oven for 2 hours. After washing with H_2O and ethanol carefully, ZHC nanodisk array deposited on TiO_2/FTO substrate was sintered in air at 500°C for 4 hours, to convert ZHC to ZnO nanoporous disk.

TiO_2 NPs slurry was prepared by grinning TiO_2 commercial nanoparticles (P90, Degauss Co.) 0.5 g, H_2O 2.5g, PEG 20000 0.25 g in porcelain mortar. The ZnO-TiO_2 hybrid film was prepared by the doctor blade method, and the ZnO nanoporous disk array grown on TiO_2/FTO substrate was used. To achieve a specific thickness of the film, two layers of TiO_2 slurry were applied. The dried hybrid cell was sintered at 450°C in air for 30 minutes.

The sensitization of photoanode films and the fabrication of the cells were similar to those described in Section 2.1, except that the sensitizing time was prolonged to 24 hours.

Figure. 7(a) illustrated SEM images of ZHC nanodisk array deposited on TiO_2/FTO substrate. It can be seen that as-deposited ZHC exhibit rather regular hexagonal disk shape, with the size of ~ 10 um. The distribution of ZHC disks on substrate is sparse, satisfying the "low-content" requirement of ZnO in the hybrid photoanode film. After annealing at 500°C, ZHC disks were transformed into ZnO with typical nanoporous structure (as shown in Figure 7(b)), while the sheet structure (~100 nm in thickness) was maintained. Figure 7 (c) and (d) showed SEM images of the hybrid films based on this sparse nanoporous ZnO disk array. We can see that the morphology of the hybrid film on the surface and the cross section was rather smooth and uniform, with little difference from the traditional pure TiO_2 film (Gao, 2007). In addition, ZnO sheet like structures can not be found in either the surface or the cross section due to the low content of ZnO in the hybrid film.

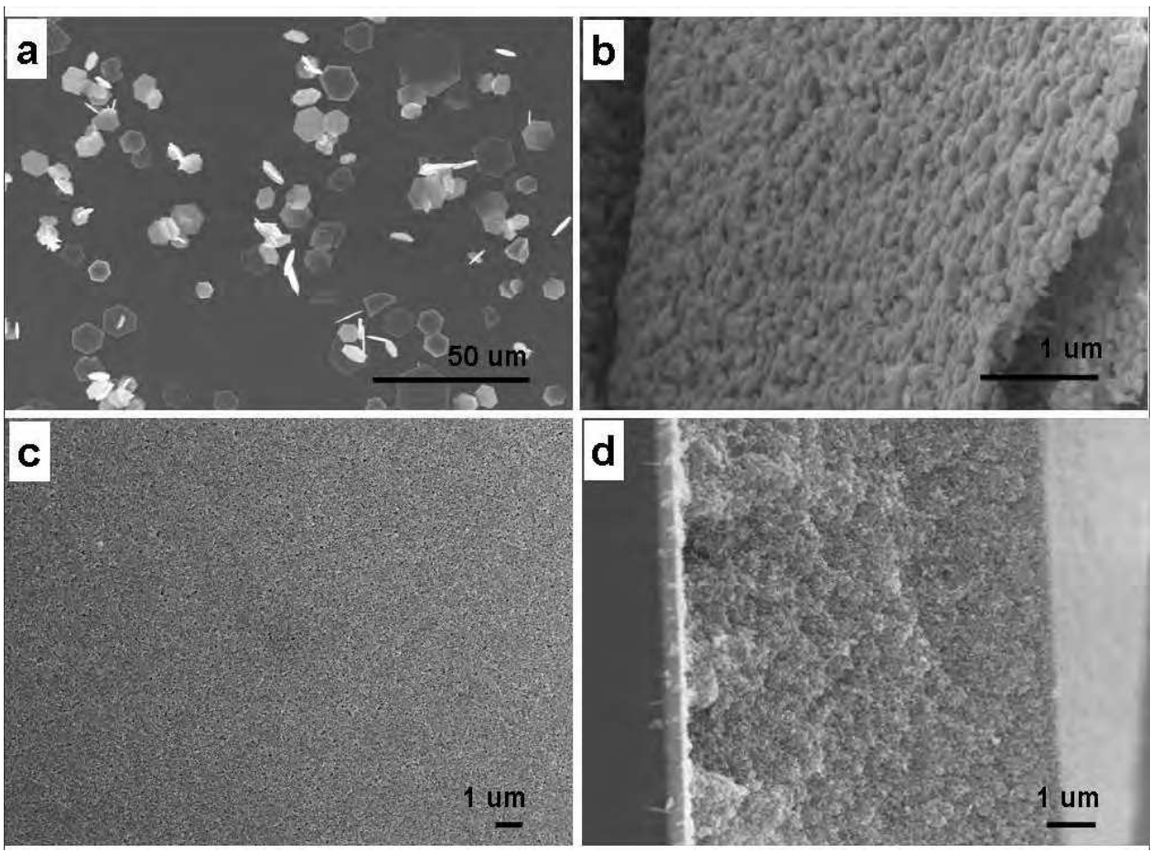

Fig. 7. FESEM images of (a) ZHC disk array and (b) ZnO nanoporous disk transformed from ZHC via calcinations at 500°C; FESEM images of ZnO-TiO_2 hybrid film based on sparse nanoporous ZnO disk array. (c) Surface and (d) cross section.

Figure 8 (left) gave the optical transmittance spectra of FTO substrate, pure TiO_2 film and the hybrid film. Results indicate that in the wavelength rage of 470-800 nm, the hybrid film possesses relatively lower transmittance than the pure TiO_2 film, while in the wavelength band of 300-470 nm, the transmittance of the hybrid film is higher. The reduced transmittance in the higher wavelength band of the hybrid film may be related to the scattering effects of the large ZnO disk in the film. In view of the maximum absorption of N719 dye molecules located at ~ 525 nm (Figure 4), the scattering of ZnO nanoporous disks to the incident light has positive influence on the performance of the hybrid cells. The reduced transmittance in the lower band of the pure TiO_2 film may be related to the increased agglomeration of TiO_2 NPs, which can induce the larger secondary particles and the higher scattering effects in the lower wavelength range. In contrast, the presence of large-size ZnO sheet may reduce the agglomeration phenomena to some extent, thus exhibiting higher transmittance.

Figure 8 (right) gave I-V curves of pure TiO_2 NPs cell and ZnO nanodisk array – TiO_2 NPs hybrid cell under AM 1.5 illumination (100 mW/cm²). It can be seen that the cell based on the hybrid film possesses much higher photocurrent density than TiO_2 NPs cell, increasing from 7.84 mA/cm² to 11.70 mA/cm². Also the improvements in the photovoltage and the fill factor of the hybrid cell are observed. As a result, the total conversion efficiency changes from 3.07% to 5.19%, increased by up to 60%.

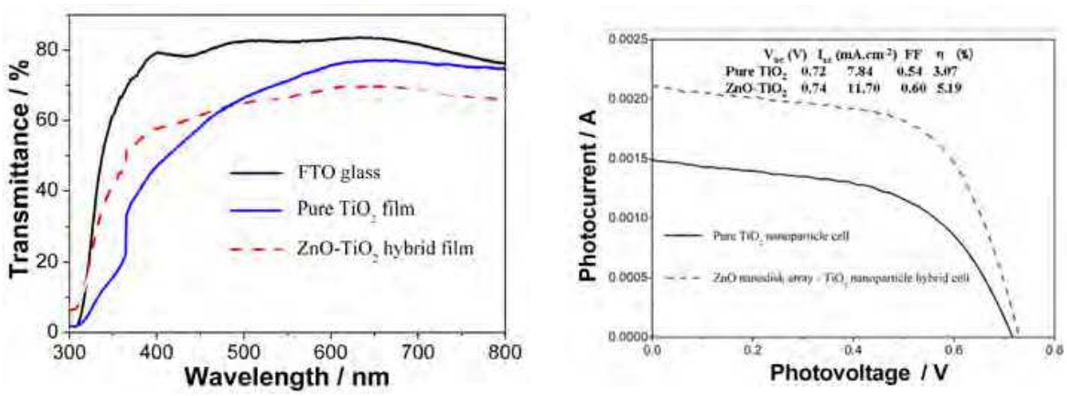

Fig. 8. The optical transmittance spectra (left) of pure TiO_2 NPs film and ZnO-TiO_2 hybrid film deposited on FTO substrate; I-V curves (right) of pure TiO_2 NPs cell and ZnO nanodisk array – TiO_2 NPs hybrid cell under AM 1.5 illumination (100 mW/cm²). The active area is 0.27 cm² for pure TiO_2 cell and 0.18 for ZnO-TiO_2 hybrid cell.

The reason for the efficiency improvement in the hybrid cell compared with NPs-based cell was analyzed by AC impedance under the illumination condition and open-circuit voltage decay (OCVD) analysis under the dark condition.

Figure 9 (left) showed Nyquist plots of the hybrid and pure photoanode, and the lower table gave the simulation results according to the physical model given in the inset. Two arcs can be clearly identified in the Nyquist plot for each sample. The left (high frequency) arc corresponds to the charge transfer process at the Pt counter electrode (R_{ct1}). The right large arc arises from the charge transport at the TiO_2/dye/electrolyte interface (R_{ct2}). The right small arc is related to the Warburg diffusion process of I^-/I_3^- in the electrolyte, which is not discussed in this work. The overall series resistance of the cell (R_s) is the resistance measured when electrons are transported through the device in the high-frequency range exceeding10^5

Hz. By simulated calculation following the equivalent circuit, we can obtain the calculated value of R_s, R_{ct1}, and R_{ct2} for each sample. Results show that the hybrid film exhibits obviously lower R_s, R_{ct1}, and R_{ct2} than the pure TiO_2 film, indicating that the overall series resistance, the resistance at the Pt/electrolyte interface and at the TiO_2/dye/electrolyte interface in the hybrid cell is lower than the traditional TiO_2 NPs cell.

Figure 9 (right) showed OCVD curves of the hybrid and pure photoanode. While the pure TiO_2 cell exhibits rapid voltage decrease after the turning off of the illumination, the hybrid cell has much slower decay behavior, indicating that the photo-induced electron-hole recombination rate in the hybrid film is lower than the pure TiO_2 cell.

We believe the reduced overall resistance, the interfacial resistance and the electron-hole recombination rate is responsible for the obvious improvement in the total conversion efficiency in the hybrid cell.

In brief, we prepared ZnO-TiO_2 hybrid photoanode film based on sparse ZnO nanoporous disk array grown on TiO_2/FTO substrate. Though the obvious change in the microstructure of the film could not be observed, the hybrid film possessed increasing scattering effects in the wavelength range of 470-800 nm, which was beneficial to the light absorption of the dye molecules. Also the integration of ZnO nanoporous disk into TiO_2 NPs film resulted in the decrease of the overall series resistance and the resistance at the Pt/electrolyte interface and at the TiO_2/dye/electrolyte interface. As a result, the conversion efficiency was improved by 60%, indicating the great potential of the sparse ZnO nanoporous disk array in the field of hybrid DSC photoanodes.

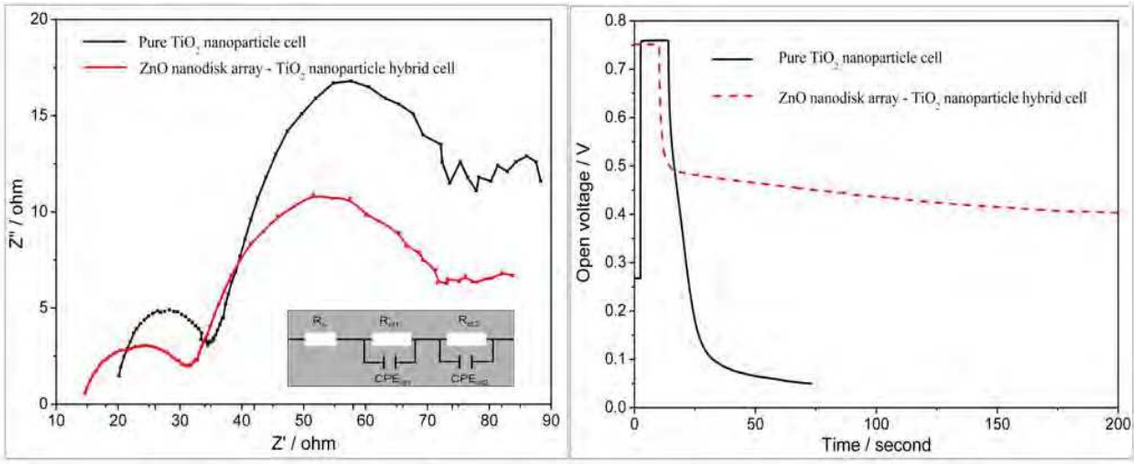

	R_s (Ω)	CPE_{ct1} ($uFS^{\alpha-1}$)	R_{ct1} (Ω)	α_{ct1}	CPE_{ct2} ($uFS^{\alpha-1}$)	R_{ct2} (Ω)	α_{ct2}
Pure TiO_2	**18.54**	6.45E-5	**17**	0.63	0.00176	**46.50**	0.78
ZnO-TiO_2	**12.21**	1.55E-4	**12**	0.60	0.00243	**28.00**	0.82

Fig. 9. Nyquist plots (left) and open-circuit voltage decay plots of pure TiO_2 NPs cell and ZnO nanodisk array – TiO_2 NPs hybrid cell. The attached table illustrates EIS parameters calculated from the given equivalent circuit.

4. ZnO nanoporous disk powder/TiO_2 NPs hybrid photoanodes

The disadvantage for the hybrid photoanode between ZnO array (both the nanoporous disk array and the nanowire array) and TiO_2 NPs lies in the difficulties in controlling the precise content of ZnO in the hybrid film, which is a crucial parameter for any composite material. Also, the distribution of ZnO array in the hybrid film may be not uniform, and difficult to control. Therefore, in this section, we attempted to blend ZnO nanoporous disk in the powder form into TiO_2 slurry, and prepared a uniform hybrid film via the doctor-blade technique. By this method, we can examine the effects of ZnO content in the hybrid film on the microstructure and properties of photoanode, and find an optimal composition for ZnO-TiO_2 hybrid photoanodes.

The powder of ZnO nanoporous disks was synthesized by the pyrolysis of chemical bath deposited ZHC nanodisks. Two types of TiO_2 NPs were selected, i.e., the commercial P25 TiO_2 and the hydrothermal TiO_2 NPs following the procedure described in Ref (Ito et al., 2008).

4.1 Hybrid photoanodes based on P25 TiO_2 NPs

Layered ZHC was prepared by the chemical bath deposition method. Typically, aqueous solutions of 20 ml $ZnCl_2$ (0.2 mol/l), 20 ml hexamethylenetetramine (HMT) (0.2 mol/l), and 40 ml ethanol were mixed together and heated to 70°C in oven for 2 hours, resulting in the white precipitation of ZHC. After centrifuging and drying, the powders were annealed at 500°C in a tube furnace in air for 18 hours to convert ZHC into ZnO.

Film electrodes for DSCs were deposited onto FTO substrate via TiO_2 or TiO_2/ZnO slurry by the doctor blade technique. For P25 TiO_2 NPs, the TiO_2 slurry was prepared using the mixed suspension of TiO_2 NPs (P25) (0.5 g) and PEG-1000 (0.25 g). The TiO_2/ZnO hybrid electrodes were made by using the mixed suspension of P25, PEG and ZnO disk powder, with the weight percentages of ZnO being 0 (S1), 0.5% (S3) and 1% (S2). The electrodes were sintered at 450°C for 120 min. The detail preparation process of the hybrid film was illustrated in Figure 10.

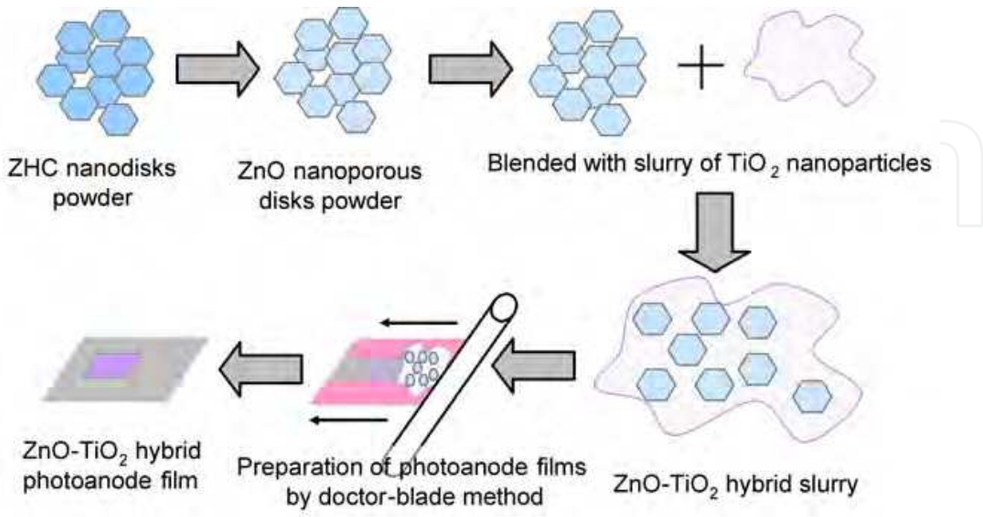

Fig. 10. Schematic of the preparation process of ZnO/TiO_2 hybrid photoanodes based on nanoporous ZnO disk powder and TiO_2 nanoparticles.

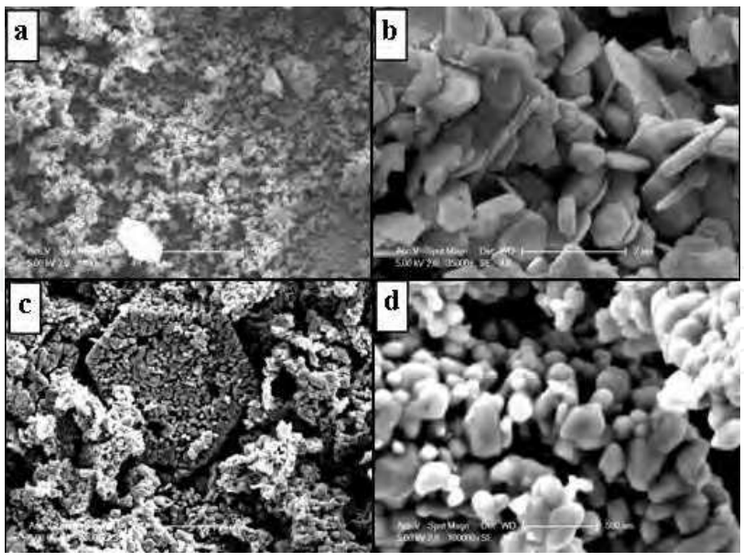

Fig. 11. SEM images of as-prepared ZHC powders and ZnO nanoporous disk after annealing at 500°C: (a) Low magnification morphology of ZHC powder; (b) Typical ZHC disks; (c) Low magnification morphology of ZnO nanoporous disks; (d) Enlarged view of nanoporous structure. (Reproduced from Ref (Gao et al., 2009))

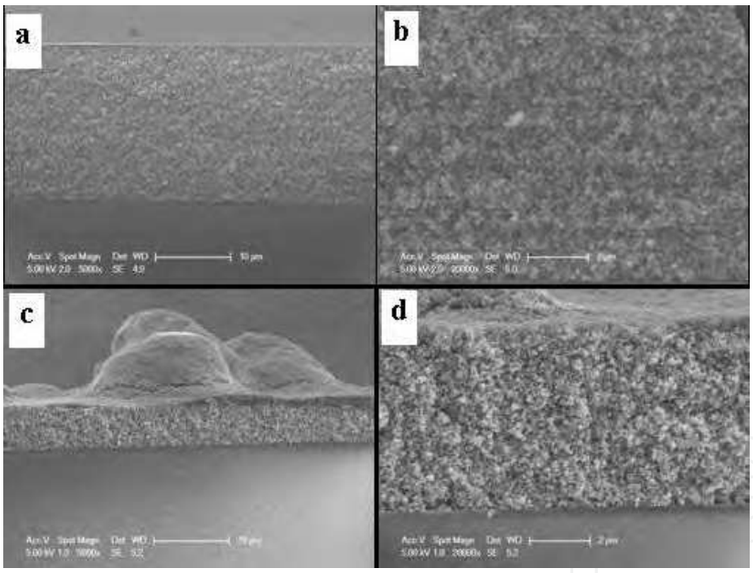

Fig. 12. SEM images of the cross section of TiO_2 film (a-b) and ZnO-TiO_2 hybrid film (c-d) prepared on glass substrate. (a) and (c): low magnification; (b) and (d): high magnification. (Reproduced from Ref (Gao et al., 2009))

The annealed electrodes were stained by N719 dye by soaking them in a 0.5 mmol/l solution of N719 for 12 hours. FTO glass substrates were coated by Pt catalyst layer by decomposing $H_2PtCl_6{\cdot}6(H_2O)$ at 400°C, and were used as the counter electrode. The working electrode and the counter electrode were cohered together by surlyn 1702 hot melt foil. The electrolyte, consisted of 0.05 M I_2, 0.1 M LiI and 0.5 M tertbutylpyridine in acetonitrile, was filled into the cell from the hole in the counter electrode.

Figure 11 gave SEM images of as-prepared ZHC disks and nanoporous ZnO disks obtained by sintering. As-prepared ZHC possesses obvious disk-like feature, with the side length of 500-1000 nm and the thickness of 100-300 nm in average. After annealing, ZnO disks with the nanoporous feature were obtained, with the pore size ranging from 50-200 nm. In addition, the linking between neighboring ZnO particles in each disk can be clearly observed, which is expected to provide good electron transport in DSCs.

Figure 12 showed the cross-section morphologies of the pure TiO_2 film and 1%ZnO/TiO_2 hybrid film. While the pure TiO_2 film shows a uniform surface morphology and typical nanoporous structure with a thickness of ~20 μm, the hybrid film possesses a rough surface with large humps of ~10 μm (Fig.12 c) and lower thickness (~6 μm). The results indicate that even a small amount of ZnO powder blended in TiO_2 slurry can change the microstructure and thickness of the film electrodes significantly, which may be related to the change of the slurry viscosity during the preparation process. The presence of large ZnO particles (several μm in size) in the hybrid slurries may hamper the free flow of the TiO_2 slurry, thus resulting in the formation of large humps on the surface and the higher internal roughness

The optical transmittance spectra (Figure 13 (left)) of the TiO_2 and ZnO/TiO_2 hybrid films shows that both the pure and hybrid films exhibit strong scattering effects on the incident light in the visible and near infrared band. Compared with the pure TiO_2 film electrode, the hybrid film electrodes show much lower transmittance in the wavelength range of 500-1100 nm, indicating that a very small amount of ZnO disks can exert significant effects on the optical properties of the photoanode.

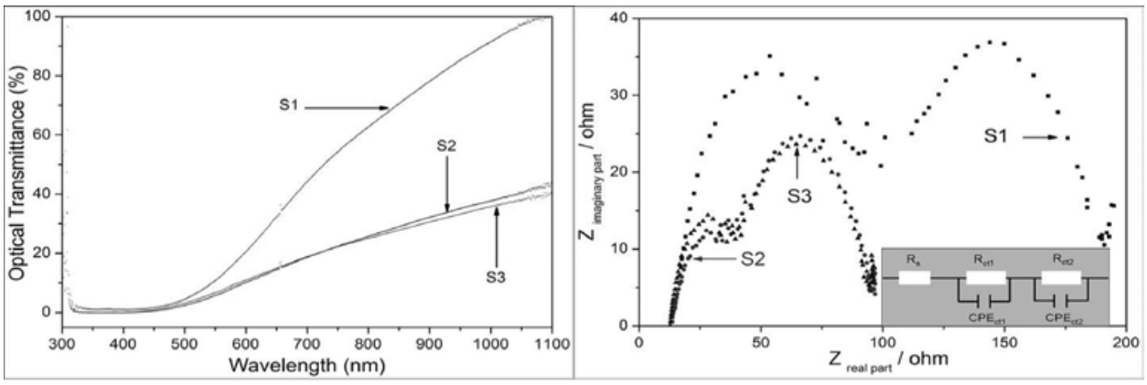

	R_s ($\Omega .cm^{-2}$)	CPE_{ct1} ($uFcm^{-2}S^{\alpha-1}$)	R_{ct1} (Ωcm^{-2})	α_{ct1}	CPE_{ct2} ($uFcm^{-2}S^{\alpha-1}$)	R_{ct2} (Ωcm^{-2})	α_{ct2}
S1	14.69	49.65	74.46	0.85	311.2	108.10	0.71
S2	13.00	223.10	57.59	0.82	8.36	26.29	0.89
S3	13.51	229.00	56.99	0.84	31.22	27.28	0.76

Fig. 13. Optical transmittance (left) of TiO_2 film (S1) and ZnO/TiO_2 hybrid film on FTO glass substrate, with ZnO percentage of 1% (S2) and 0.5% (S3), and electrochemical impedance spectra (right) of the DSCs based on TiO_2 electrode (S1) and ZnO-TiO_2 hybrid electrodes (S2 and S3). The attached table illustrates EIS parameters calculated from the given equivalent circuit. (Reproduced from Ref (Gao et al., 2009))

Figure 13 (right) showed the impedance spectra of DSCs using TiO_2 and ZnO/TiO_2 hybrid photoanodes. Results show that, both hybrid cells exhibit lower R_s, R_{ct1}, and R_{ct2} than those of the pure TiO_2 cell (S1), indicating that the incorporation of ZnO in the photoanode can decrease the overall series resistance of device significantly and facilitate the interfacial charge transport in both Pt/electrolyte and TiO_2/dye/electrolyte interface. The reason for this improvement may be the combination of the high electron transport nature of one-dimensional ZnO materials (Martinson et al., 2006), the large particle size and the network structure of ZnO disk.

Figure 14 revealed I-V curves of DSCs with TiO_2 and ZnO-TiO_2 hybrid films. The overall efficiencies of three cells are in the order of S3>S2>S1. While the cell using pure TiO_2 electrode (S1) exhibits the lowest efficiency of 1.1%, the cells with 0.5% and 1% ZnO-TiO_2 hybrid electrodes show higher efficiency of 2.7% and 2.3%, improved by 145% and 109%, respectively. Two hybrid cells exhibit similar V_{oc} but significantly higher I_{sc} and higher fill factor than pure TiO_2 cell, indicating that the improvement in the photocurrent density and fill factor is the main reason for the efficiency improvement. Also, the concentration of ZnO in the hybrid film should be no higher than 1% in this case, which is consistent with our previous observation in the hybrid film based on the sparse ZnO nanoporous disk array (Section 3) and results of other researchers on the DSCs with ZnO nanorod-TiO_2 hybrid electrode (Kang et al., 2007).

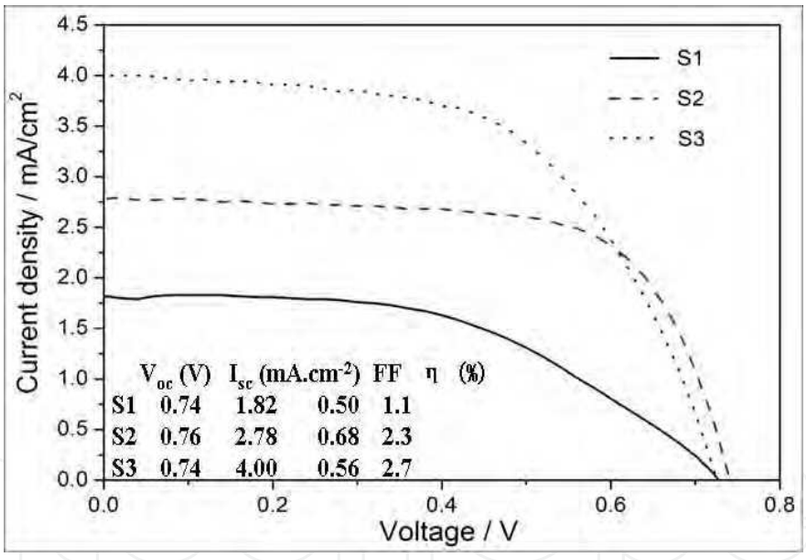

Fig. 14. The I–V characteristic curves of DSCs based on TiO_2 electrode (S1) and ZnO/TiO_2 hybrid electrode with ZnO percentage of 1% (S2) and 0.5% (S3). (Reproduced from Ref (Gao et al., 2009))

In summary, we have successfully demonstrated that ZnO nanoporous disk prepared from layered zinc based compound ZHC can be used to improve the efficiency of TiO_2 photoanodes effectively. The direct incorporation of ZnO nanodisk powder into TiO_2 slurry combined with the doctor-blade technique was proved an effective way to prepare the hybrid films. Results showed that even a small amount of ZnO incorporation in the TiO_2 film (≤1%) can significantly influence the microstructure, optical and electrical properties. The rougher inner microstructure, the enhanced light-scattering effect on the visible and

infrared light region, and the higher interfacial charge-transport rate were responsible for the improved efficiency in the hybrid photoanodes when compared with the pure TiO_2 film.

4.2 Hybrid photoanodes based on hydrothermal TiO_2 NPs

In this section, TiO_2 hydrothermal NPs were used as the source of TiO_2 for the preparation of the hybrid film. ZnO-TiO_2 hybrid slurry was prepared by adding specific amount of ZnO nanoporous disk powder into TiO_2 NPs slurry. TiO_2 NPs were prepared via the hydrothermal method and the slurry containing TiO_2 (18% by weight), ethyl cellulose (9%) and terpineol (73%) was prepared following Ref (Ito et al., 2008). ZnO nanoporous disk powder with the weight percentage of 0.5%-2% (compared with TiO_2) was blended into the slurry before the evaporation of ethanol via rotate-evaporator. Due to the acid-dissolute nature of ZnO materials, the pH value of TiO_2 slurry should be controlled at neutral or weak alkaline range.

ZnO-TiO_2 hybrid photoanodes were prepared by the doctor-blade technique using the hybrid slurry. Conductive FTO glass coated by a thin TiO_2 layer (deposited by the hydrolysis of 40 mM $TiCl_4$ aqueous solution at 70°C) was used as the substrate. The sensitization of the photoanode film and the fabrication of the cells were similar to the procedure described in Section 2.2.

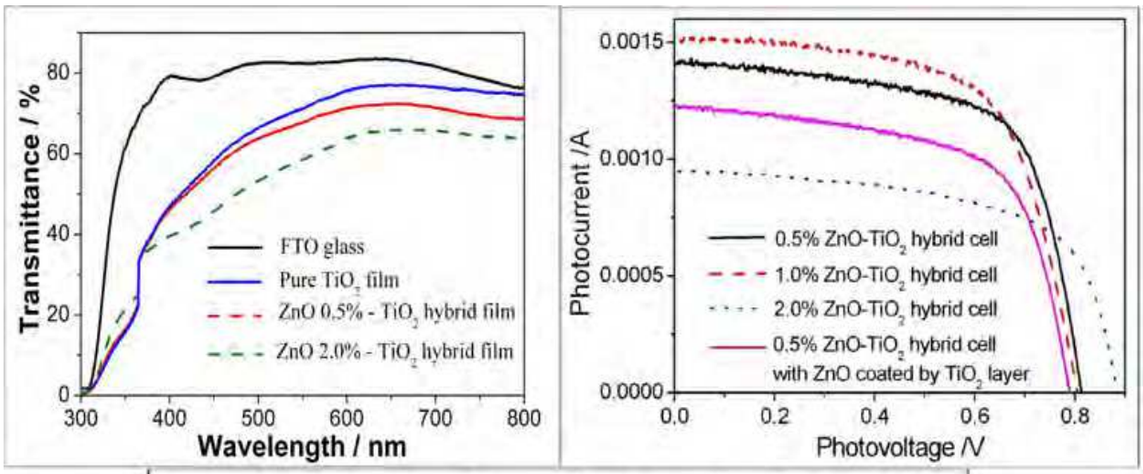

	V_{oc} (V)	I_{sc} (mA.cm^{-2})	FF	η (%)
0.5%ZnO-TiO_2	0.81	5.19	0.68	2.84
1.0%ZnO-TiO_2	0.805	5.52	0.66	2.94
2.0%ZnO-TiO_2	0.89	3.52	0.62	1.94
0.5%ZnO-TiO_2 with ZnO coated	0.79	4.56	0.63	2.29

Fig. 15. Optical transmittance (left) of ZnO-TiO_2 hybrid film deposited on FTO substrate, and I-V curves (right) of ZnO – TiO_2 hybrid cells based on different ZnO contents (0.5-2% by weight) under AM 1.5 illumination (100 mW/cm^2). The active area is 0.27 cm^2 for all cells.

SEM analysis (not shown here) indicates that the microstructure of the hybrid film was similar to that of pure TiO_2 film, different from the results in P25 slurry (Section 4.1). We think this difference may be resulted from the solvent of the slurry. In P25 based hybrid

slurry, water is the dispersant, and the presence of large-size ZnO disk may exert significant influences on the viscosity of the slurry, thus modifying the microstructure of the hybrid film. In the hydrothermal TiO_2 hybrid slurry, organic terpineol was used as the dispersant, which possessed much higher viscosity than water. So the presence of a very small percentage of ZnO disks in the slurry had only minor influences on the viscosity and other physical properties of the hybrid slurry. Correspondingly, the microstructure of the hybrid film differed little from the pure one.

Figure 15 (left) showed optical transmittance spectra of ZnO-TiO_2 hybrid film deposited on FTO substrate. Different from microstructure results, the hybrid films exhibit obviously lower transmittance than the pure TiO_2 film in the visible-near infrared wavelength, which can be ascribed to the scattering effects of ZnO disks dispersed uniformly in the film. As mentioned above, this scattering behavior is beneficial to the absorption of N719 dye molecules. Also the hybrid film with 2% ZnO exhibits higher scattering effects than the one with 0.5% ZnO.

I-V curves given in Figure 15 (right) indicate that the photoanode with 1% ZnO possesses the highest efficiency compared with 0.5% ZnO and 2% ZnO hybrid films. While the cell parameters of the cells based on 0.5% and 1%ZnO are similar, the cell with 2%ZnO shows much less photocurrent density, which may account for the main fall in the efficiency. Also we were trying to coat a thin TiO_2 layer on ZnO nanoporous disk before its incorporation into TiO_2 slurry via the sol-gel method. Results show that this coating is not helpful in this case, maybe resulted from the reduced surface area in ZnO nanoporous disk due to TiO_2 coating. Further and in-depth investigation in this direction is required.

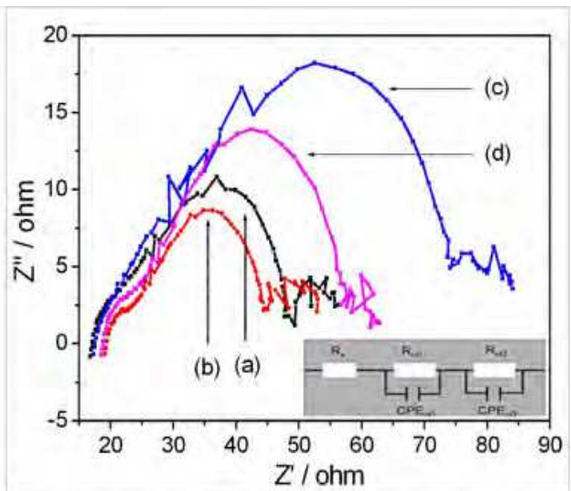

	R_s (Ω)	CPE_{ct1} (uFS^{s-1})	R_{ct1} (Ω)	a_{ct1}	CPE_{ct2} (uFS^{s-1})	R_{ct2} (Ω)	a_{ct2}
(a)	17.4	0.0015	10.0	0.7	0.004	21.5	0.9
(b)	19.4	0.003	6.5	0.7	0.0185	19.1	0.9
(c)	17.5	0.0025	14.0	0.7	0.008	44.0	0.85
(d)	18.8	0.0015	9.0	0.7	0.004	30.0	0.9

Fig. 16. Nyquist plots of ZnO nanodisk – TiO_2 NPs hybrid cells with ZnO content in hybrid slurry by weight of (a) 0.5%, (b) 1.0%, (c) 2.0%), and (d) 0.5% (ZnO disks were coated by a thin TiO_2 layer via sol-gel technique). The table illustrates EIS parameters calculated from the given equivalent circuit.

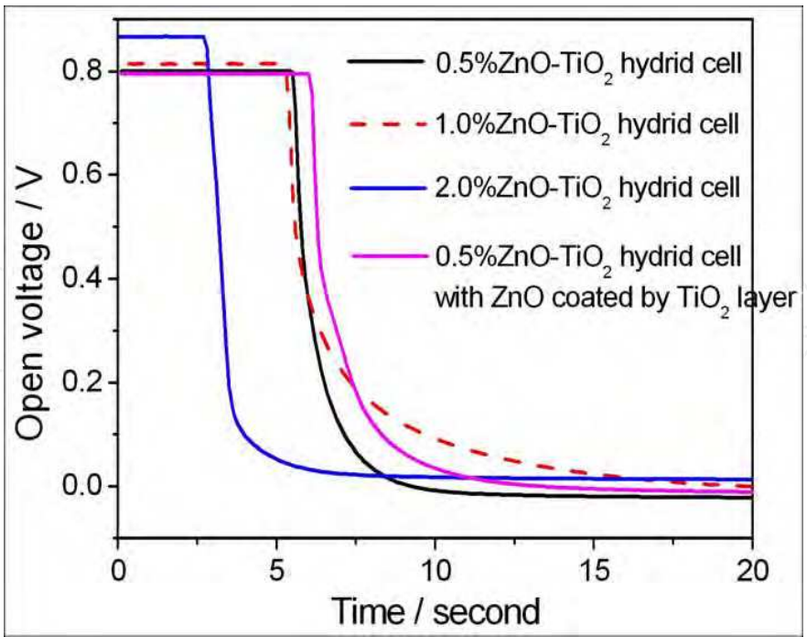

Fig. 17. Open-circuit voltage decay plots of ZnO nanodisk – TiO_2 NPs hybrid cells with different ZnO content in hybrid slurry by weight (0.5%-2.0%).

Figure 16 illustrated Nyquist plots of ZnO-TiO_2 hybrid cells obtained from EIS analysis. From the results of simulation, we can see that the hybrid cell with 1%ZnO content possesses the lowest resistance at Pt/electrolyte interface and at TiO_2/dye/electrolyte interface. The resistance at two interfaces increases when the content of ZnO in hybrid film is either lower or higher than 1%. In special, for the hybrid film with 2% ZnO content, the resistance at both interfaces is higher than that of film with 1% or 0.5% ZnO content. Also for the film with 0.5% ZnO coated with a thin TiO_2 layer, the resistance at the TiO_2/dye/electrolyte interface and the overall series resistance were increased, thus resulted in the reduction in the total conversion efficiency. In general, we can derive a linear relationship between the interfacial resistance obtained from EIS analysis and the overall conversion efficiency of the hybrid cell.

Figure 17 showed OCVD plots of the hybrid cell with different ZnO content. Results show that 1%ZnO-TiO_2 hybrid cell exhibits the slowest voltage decay rate among all four cells, indicating the lower recombination rate, which is consistent with its high conversion efficiency. Also the coating of a thin TiO_2 layer on ZnO nanoporous disk via sol-gel technique can slightly improve the recombination properties of the hybrid cell, which is beneficial to the improvement of the efficiency. However, other consequences induced by the coating, possibly the blocking of the nanopore and the decrease of the surface area, resulted in the reduction of the overall efficiency at last.

For ZnO-TiO_2 hybrid cell, it is important to discuss the effects of the treatment of the photoanode film in $TiCl_4$ aqueous solution. ZnO is intrinsically an amphoteric oxide, which can be dissolved in $TiCl_4$ aqueous solution with the strong acid nature. So it should be very careful in treating ZnO-TiO_2 hybrid films in $TiCl_4$ solutions. Figure 18 illustrated I-V curves of TiO_2 and ZnO-TiO_2 film with and without $TiCl_4$ treatment. Results show that the

incorporation of ZnO into TiO_2 can improve the efficiency from 3.5% to 3.98% before the $TiCl_4$ treatment. However, after the treatment, the efficiency of the hybrid film decreases to 3.2%, while the efficiency of the pure TiO_2 film increases to 6.38%. The dissolution of ZnO dispersed uniformly in the hybrid film may be underlying reason for the efficiency reduction. On the other hand, the $TiCl_4$ treatment is a very powerful method to improve the efficiency of the pure TiO_2 cell. So it is necessary to develop an alternative treatment method in a neutral aqueous solution, which has minor influence on the structure of ZnO. Other methods may be also helpful including the protective coating technique on ZnO nanoporous disks by thin TiO_2 layer which can resist the corrosion of acid. However, when the protective coating technique is adopted, one has to be careful in avoiding the blocking of the nanopore present in ZnO nanostructures.

In summary, this section discussed the preparation of ZnO-TiO_2 hybrid photoanode films based on ZnO nanoporous disk powder and hydrothermal TiO_2 NPs. An optimal ZnO content of ~1% in the hybrid film was observed, with the total conversion efficiency of ~2.94%. While the efficiency improvement in the hybrid cell was realized when compared with the pure TiO_2 film when no $TiCl_4$ treatment was performed, the decrease in the efficiency in the hybrid film after the $TiCl_4$ treatment indicated the sensitivity of the hybrid system. The development of other treatment methods suitable for ZnO-TiO_2 hybrid system or other protective means may afford the further direction in this field.

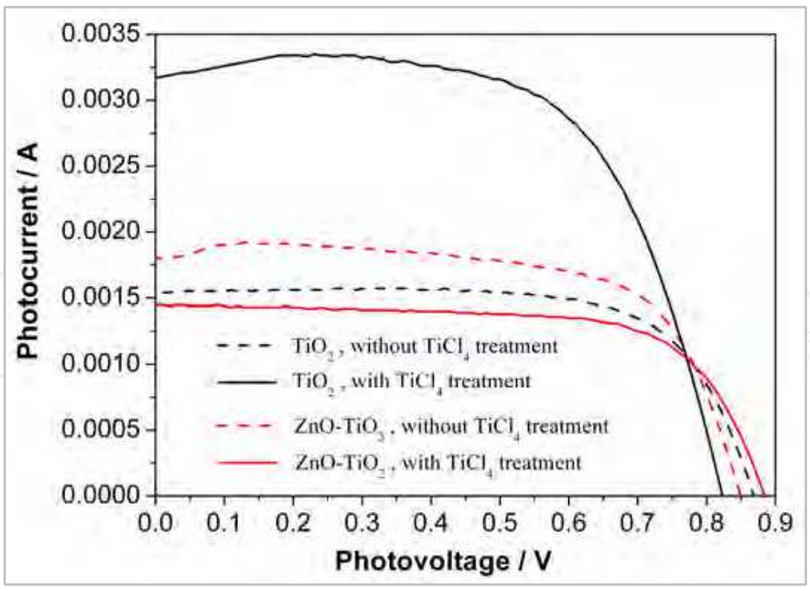

Fig. 18. I-V curves of TiO_2 NPs-based cell and ZnO–TiO_2 hybrid cells under AM 1.5 illumination (100 mW/cm²), illustrating the effects of $TiCl_4$ treatment.

5. Conclusion

In summary, the chapter started with a general review on the ordered TiO_2 and ZnO photoanode and the hybrid photoanode, outlining a brief picture on the status of the ordered photoanode in the field of DSCs. Then focusing on the ZnO-TiO_2 hybrid photoanodes, four type of ZnO nanostructure (including dense and sparse nanowire array, sparse nanoporous disk array, and nanoporous disk powder) and three type of TiO_2 nanoparticles (including P25, P90, and home-made hydrothermal nanoparticles) were used to prepare various hybrid films. Results show that, in general, the integration of ZnO with TiO_2 is a powerful means to improve the efficiency of the photoanode of DSCs, with the improvement up to 150%. However, one has to take great care in realizing the ideal hybrid structures. The content of ZnO in the hybrid film has to be maintained at a low level (e.g. ~1% by weight) in order to obtain a positive effect, which means that sparse and thin nanowire array or nanodisk array instead of the dense array is preferred. Also great care has to be taken during the $TiCl_4$ treatment of the ZnO-TiO_2 hybrid photoanode or the protective coating of ZnO nanostructures, preventing the destruction to the microstructure of ZnO nanostructures. Though at the current stage the overall conversion efficiency of the hybrid cell has not overpassed the highest level of the pure TiO_2 cell, it represents a very powerful and important technical route to optimize the microstructure and the performance of the ordered photoanode. We believe, by the continuous efforts of the forthcoming researchers, the hybrid semiconductor photoanodes with ordered structures will eventually shed the light to the DSCs with the breakthrough efficiency.

6. Acknowledgment

This work is supported by the 973-project (Grant no. 2009CB623304) of Ministry of Science and Technology of China and the Basic Research Program (Grant no. 51072214, 51002174) of National Natural Science Foundation of China.

7. References

Brown, P.; Takechi, K. & Kamat, P. V. (2008). Single-Walled Carbon Nanotube Scaffolds for Dye-Sensitized Solar Cells. *J. Phys. Chem. C,* Vol. 112, No. 12, pp. 4776-4782.

Chou, T. P.; Zhang, Q. F.; Fryxell, G. E. & Cao, G. Z. (2007). Hierarchically Structured ZnO Film for Dye-Sensitized Solar Cells with Enhanced Energy Conversion Efficiency. *Adv. Mater.,* Vol. 19, No. 18, pp. 2588-2592.

Gan, X. Y.; Li, X. M.; Gao, X. D.; Zhuge, F. W. & Yu, W. D. (2007). ZnO Nanowire/TiO_2 Nanoparticle Photoanodes Prepared by the Ultrasonic Irradiation Assisted Dip-coating Method. *Thin Solid Films.* Vol. 518, No. 17, pp. 4809–4812.

Gao, X. D.; Li, X. M.; Yu, W. D.; Qiu, J. J. & Gan, X. Y. (2007). Preparation of Nanoporous TiO_2 Thick Film and Its Photoelectrochemical Properties Sensitized by Merbromin. *J. Inorg. Mater.,* Vol. 22, No.6, pp. 1079-1085.

Gao, X. D.; Gao, W.; Yan, X. D.; Zhuge, F. W.; Bian, J. M. & Li, X. M. (2009). ZnO Nanoporous Disk-TiO_2 Nanoparticle Hybrid Film Electrode For Dye-Sensitized Solar Cells. *Funct. Mater. Lett.*, Vol. 2, No.1, pp. 27-31.

Grätzel M. (2001). Photoelectrochemical cells. *Nature,* Vol. 414, No. 6861, pp. 338-344.

Grätzel M. (2006). Photovoltaic Performance and Long-Term Stability of Dye-Sensitized Mesoscopic Solar Cells. *C. R. Chimie,* Vol. 9, No. 5/6, pp. 578-583.

Guldin, S.; Huttner, S.; Kolle, M.; Welland, M. E.; Muller-Buschbaum, P.; Friend, R. H.; Steiner, U. & Te´treault N. (2010). Dye-Sensitized Solar Cell Based on a Three-Dimensional Photonic Crystal. *Nano Lett.,* Vol. 10, No. 7, pp. 2303–2309.

Hosono, E.; Fujihara, S.; Honma, I. & Zhou, H. (2005). The Fabrication of an Upright-Standing Zinc Oxide Nanosheet for Use in Dye-Sensitized Solar Cells. *Adv. Mater.,* Vol. 17, No. 17, pp. 2091–2094.

Ito, S; Murakami, T. N.; Comte, P.; Liska, P.; Grätzel, C.; Nazeeruddin, M. K. & Grätzel M. (2008). Fabrication of Thin Film Dye Sensitized Solar Cells with Solar to Electric Power Conversion Efficiency Over 10%. *Thin Solid Films*, Vol. 516, No. 14, pp. 4613-4619.

Kang, S. H.; Kim, J. Y.; Kim, Y.; Kim, H. S. & Sung, Y. E. (2007). Surface Modification of Stretched TiO_2 Nanotubes for Solid-State Dye-Sensitized Solar Cells. *J. Phys. Chem. C,* Vol. 111, No. 26, pp. 9614-9623

Kang, S. H.; Choi, S. H.; Kang, M. S.; Kim, J. Y.; Kim, H. S.; Hyeon, T. & Sung, Y. E. (2008). Nanorod-Based Dye-Sensitized Solar Cells with Improved Charge Collection Efficiency. *Adv. Mater.,* Vol. 20, No.1, pp. 54 -58.

Ku, C. H.; Yang, H. H.; Chen, G. R. & Wu, J. J. (2008). Wet-Chemical Route to ZnO Nanowire-Layered Basic Zinc Acetate/ZnO Nanoparticle Composite Film. *Cryst. Growth Des.,* Vol. 8, No. 1, pp. 283-290.

Law, M.; Greene, L. E.; Johnson, J. C.; Saykally, R. & Yang P. (2005). Nanowire dye-sensitized solar cells. *Nature Materials,* Vol. 4, No. 6, pp. 455-459.

Law, M.; Greene, L. E.; Radenovic, A.; Kuykendall, T.; Liphardt, J. & Yang, P. (2006). ZnO-Al_2O_3 and ZnO-TiO_2 Core-Shell Nanowire Dye-Sensitized Solar Cells. *J. Phys. Chem. B,* Vol. 110, No. 45, pp. 22652-22663.

Lee, K. M.; Hu, C. W.; Chen, H. W. & Ho, K. C. (2008). Incorporating Carbon Nanotube in a Low-Temperature Fabrication Process for Dye-Sensitized TiO_2 Solar Cells. *Solar Energy Materials & Solar Cells,* Vol. 92, No. 12, pp. 1628-1633.

Li, B.; Wang, L. D.; Kang, B.; Wang, P. & Qiu, Y. (2006). Review of Recent Progress in Solid-State Dye-Sensitized Solar Cells. *Sol. Energy Mater. Sol. Cells,* Vol. 90, No. 5, pp.549-573.

Martinson, A. B. F.; McGarrah, J. E.; Parpia, M. O. K. & Hupp, J. T. (2006). Dynamics of Charge Transport and Recombination in ZnO Nanorod Array Dye-sensitized Solar Cells. *Phys. Chem. Chem. Phys.*, Vol. 8, No. 40, pp. 4655-4659.

Martinson, A. B. F.; Jeffrey, J. W.; Elam, W.; Hupp, J. T. & Pellin, M. J. (2007). ZnO Nanotube Based Dye-Sensitized Solar Cells. *Nano Lett.*, Vol. 7, No. 8, pp. 2183-2187.

Mor, G. K.; Varghese, O. K.; Paulose, M.; Shankar, K. & Grimes C. A. (2006a). A Review on Highly Ordered, Vertically Oriented TiO_2 Nanotube Arrays: Fabrication, Material Properties, and Solar Energy Applications. *Sol. Energy Mater. Sol. Cells,* Vol. *90*, No. 14, pp. 2011-2075.

Mor, G. K.; Shankar, K.; Paulose, M.; Varghese, O. K. & Grimes, C. A. (2006b). Use of Highly-Ordered TiO_2 Nanotube Arrays in Dye-Sensitized Solar Cells. *Nano Lett.,* Vol. 6, No. 2, pp. 215-218.

Nazeeruddin, M. K.; Kay, A.; Rodicio, I.; Humpbry-Baker, R.; Müller, E.; Liska, P.; Vlachopoulos, N. & Grätzel, M. (1993). Conversion of Light to Electricity by Cis-X2bis(2,2'-bipyridyl-4,4'-dicarboxylate) Ruthenium(II) Charge-Transfer Sensitizers (X = Cl-, Br-, I-, CN-, and SCN-) on Nanocrystalline Titanium Dioxide Electrodes. *J. Am. Chem. Soc.,* Vol. 115, No.14 , pp. 6382-6390.

O'Regan B. & Grätzel M. (1991). A Low-Cost, High-Efficiency Solar Cell Based on Dye-Sensitized Colloidal TiO_2 Films. *Nature,* Vol. *353*, No. 6346, pp. 737-740.

Pang, S.; Xie, T.; Zhang, Y.; Wei, X.; Yang, M.; Wang, D. & Du, Z. (2007). Research on the Effect of Different Sizes of ZnO Nanorods on the Efficiency of TiO_2-Based Dye-Sensitized Solar Cells. *J. Phys. Chem. C,* Vol. 111, No. 49, pp. 18417-18422.

Park, K.; Zhang, Q.; Garcia, B. B.; Zhou, X. Y.; Jeong, Y. H. & Cao, G. Z. (2010). Effect of an Ultrathin TiO_2 Layer Coated on Submicrometer-Sized ZnO Nanocrystallite Aggregates by Atomic Layer Deposition on the Performance of Dye-Sensitized Solar Cells. *Adv. Mater.,* Vol. 22, No. 21, pp. 2329–2332.

Rensmo, H.; Keis, K.; Lindstrom, H.; Sodergren, S.; Solbrand, A.; Hagfeldt, A. & Lindquist, S. E. (1997). High Light-to Energy Conversion Efficiencies for Solar Cells Based on Nanostructured ZnO Electrodes. *J. Phys. Chem. B.*, Vol. 101, No. 14, pp. 2598-2601.

Rustomji, C. S.; Frandsen, C. J.; Jin, S. & Tauber, M. J. (2010). Dye-Sensitized Solar Cell Constructed with Titanium Mesh and 3-D Array of TiO_2 Nanotubes. *J. Phys. Chem. B,* Vol. 114, No. 45, pp. 14537–14543.

Tan, B. & Wu, Y. Y. (2006). Dye-Sensitized Solar Cells Based on Anatase TiO_2 Nanoparticle/Nanowire Composites. *J. Phys. Chem. B,* Vol. 110, No. 32, 15932-15938.

Wang, J. X.; Wu, C. M. L.; Cheung, W. S.; Luo, L. B.; He, Z. B.; Yuan, G. D.; Zhang, W. J.; Lee, C. S. & Lee, S. T. (2010). Synthesis of Hierarchical Porous ZnO Disklike Nanostructures for Improved Photovoltaic Properties of Dye-Sensitized Solar Cells. *J. Phys. Chem. C,* Vol. 114, No. 31, pp. 13157–13161.

Xu, C. K.; Shin, P.; Cao, L. L. & Gao, D. (2010). Preferential Growth of Long ZnO Nanowire Array and Its Application in Dye-Sensitized Solar Cells. *J. Phys. Chem. C,* Vol. 114, No. 1, pp. 125–129.

Zhang, Q.; Chou, T.; Russo, B.; Jenekhe, S. & Cao, G. (2008). Aggregation of ZnO Nanocrystallites for High Conversion Efficiency in Dye-Sensitized Solar Cells. *Angew. Chem. Int. Edt.*, Vol. 47, No. 13, pp. 2402-2406.

Zhang, W.; Zhu, R.; Ke, L.; Liu, X. Z.; Liu, B. & Ramakrishna S. (2010). Anatase Mesoporous TiO_2 Nanofibers with High Surface Area for Solid-State Dye-Sensitized Solar Cells. *Small,* Vol. 6, No. 19, pp. 2176–2182.

Zhang Q. F. & Cao G. Z. (2011). Nanostructured Photoelectrodes for Dye-Sensitized Solar Cells. *Nano Today,* Vol. 6, No. 1, pp. 91-109.

Zhu, K.; Neale, N. R.; Miedaner, A. & Frank, A. J. (2007). Enhanced Charge-Collection Efficiencies and Light Scattering in Dye-Sensitized Solar Cells Using Oriented TiO_2 Nanotubes Arrays. *Nano Lett.,* Vol. 7, No. 1, pp. 29-74.

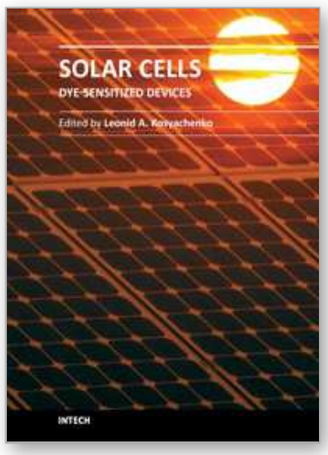

Solar Cells - Dye-Sensitized Devices
Edited by Prof. Leonid A. Kosyachenko

ISBN 978-953-307-735-2
Hard cover, 492 pages
Publisher InTech
Published online 09, November, 2011
Published in print edition November, 2011

The second book of the four-volume edition of "Solar cells" is devoted to dye-sensitized solar cells (DSSCs), which are considered to be extremely promising because they are made of low-cost materials with simple inexpensive manufacturing procedures and can be engineered into flexible sheets. DSSCs are emerged as a truly new class of energy conversion devices, which are representatives of the third generation solar technology. Mechanism of conversion of solar energy into electricity in these devices is quite peculiar. The achieved energy conversion efficiency in DSSCs is low, however, it has improved quickly in the last years. It is believed that DSSCs are still at the start of their development stage and will take a worthy place in the large-scale production for the future.

InTech Europe
University Campus STeP Ri
Slavka Krautzeka 83/A
51000 Rijeka, Croatia
Phone: +385 (51) 770 447
Fax: +385 (51) 686 166
www.intechopen.com

InTech China
Unit 405, Office Block, Hotel Equatorial Shanghai
No.65, Yan An Road (West), Shanghai, 200040, China
中国上海市延安西路65号上海国际贵都大饭店办公楼405单元
Phone: +86-21-62489820
Fax: +86-21-62489821

IntechOpen